

Article

# Improved Cycling Performance and High Rate Capacity of $\text{LiNi}_{0.8}\text{Co}_{0.1}\text{Mn}_{0.1}\text{O}_2$ Cathode Achieved by $\text{Al}(\text{PO}_3)_3$ Modification via Dry Coating Ball Milling

Feng Wang <sup>1,2,\*</sup> , Yikuan Luo <sup>2</sup>, Peng Liu <sup>2</sup>, Muhammad-Sadeeq Balogun <sup>1,\*</sup> , Jianqiu Deng <sup>2</sup>  and Zhongmin Wang <sup>2</sup> 

<sup>1</sup> College of Materials Science and Engineering, Hunan University, Changsha 410082, China

<sup>2</sup> School of Materials Science and Engineering, Guilin University of Technology, Guilin 541004, China; ykluo@139.com (Y.L.); liupeng@guet.edu.cn (P.L.); jqdeng@guet.edu.cn (J.D.); zmwang@guet.edu.cn (Z.W.)

\* Correspondence: wf@guet.edu.cn (F.W.); balogun@hnu.edu.cn (M.-S.B.)

**Abstract:**  $\text{LiNi}_{0.8}\text{Co}_{0.1}\text{Mn}_{0.1}\text{O}_2$  (NCM811) has attracted extensive attention as a promising cathode of lithium-ion batteries (LIBs) in next-generation electric vehicles, as the NCM811 sample possesses a high energy density and a price advantage. In this work, NCM811 was modified with an  $\text{Al}(\text{PO}_3)_3$  precursor using the dry ball milling method followed by heat treatment to enable commercial development both at room temperature and a higher temperature. Compared with the unmodified NCM811 sample with the capacity retention of 68.70%, after  $\text{Al}(\text{PO}_3)_3$  modification, the NCM811 sample heated to 500 °C exhibited a super capacity retention ratio of 93.88% after 200 charging–discharging cycles with the initial discharge capacity of 178.1 mAh  $\text{g}^{-1}$  at 1 C. Additionally, after  $\text{Al}(\text{PO}_3)_3$  modification, the NCM811 sample heated to 500 °C showed much improved rate performance compared to bare NCM811 at the current density of 5 C. The enhanced electrochemical performance after cycling was due to the decreased charge transfer resistance and increased  $\text{Li}^+$  transmission, which were confirmed via electrochemical impedance spectra (EIS). The NCM electrodes showed improved structural stability as layered structures after  $\text{Al}(\text{PO}_3)_3$  modification, consistent with the improved cycling performance. This work revealed that  $\text{LiNi}_{0.8}\text{Co}_{0.1}\text{Mn}_{0.1}\text{O}_2$  material with phosphide coating can be constructed using a simple ball milling method, which is feasible for obtaining high-performance electrode materials.

**Keywords:** lithium-ion battery;  $\text{LiNi}_{0.8}\text{Co}_{0.1}\text{Mn}_{0.1}\text{O}_2$  cathode;  $\text{Al}(\text{PO}_3)_3$  modification; dry ball milling; cycling stability



**Citation:** Wang, F.; Luo, Y.; Liu, P.; Balogun, M.-S.; Deng, J.; Wang, Z. Improved Cycling Performance and High Rate Capacity of  $\text{LiNi}_{0.8}\text{Co}_{0.1}\text{Mn}_{0.1}\text{O}_2$  Cathode Achieved by  $\text{Al}(\text{PO}_3)_3$  Modification via Dry Coating Ball Milling. *Coatings* **2022**, *12*, 319. <https://doi.org/10.3390/coatings12030319>

Academic Editor: Ioannis V. Yentekakis

Received: 3 February 2022

Accepted: 24 February 2022

Published: 28 February 2022

**Publisher's Note:** MDPI stays neutral with regard to jurisdictional claims in published maps and institutional affiliations.



**Copyright:** © 2022 by the authors. Licensee MDPI, Basel, Switzerland. This article is an open access article distributed under the terms and conditions of the Creative Commons Attribution (CC BY) license (<https://creativecommons.org/licenses/by/4.0/>).

## 1. Introduction

The use of new energy vehicles is rising worldwide, and lithium-ion batteries (LIBs) are widely applied as a power system to provide energy to these types of vehicles [1]. With the improvement of the quality of electric vehicles, more requirements with regard to electric vehicle mileage are made apparent, such as a high specific capacity, long life span for charge–discharge, and high energy density. The cathode material used in LIBs is the key material that restricts the endurance mileage of electric vehicles. To improve the electrochemical performance of cathode materials used in LIBs, researchers have focused on layered cathode materials of  $\text{LiNi}_x\text{Co}_y\text{Mn}_z\text{O}_2$  with higher nickel content (NCM,  $x + y + z = 1$ ,  $x > 0.6$ ) due to their high discharge capacity and price advantage [2]. With the increase in nickel content, the energy density increases in cathode materials in LIBs. The NCM811 cathode material has attracted attention due to its high capacity of more than 200 mAh  $\text{g}^{-1}$  between the charging–discharging window of 3.0–4.3 V, and it is expected to achieve a high energy density of 300 Wh  $\text{kg}^{-1}$  in the near future as a LIB cathode material [3]. Nevertheless, there are still a few intrinsic issues that need to be settled with regard to the NCM811 material. Firstly, during the synthesis and cycling process,  $\text{Ni}^{2+}$  can easily migrate into the lithium

layer as the ion radii of  $\text{Ni}^{2+}$  (0.69 Å) is similar to that of  $\text{Li}^+$  (0.76 Å). Lithium–nickel ion mixing leads to an undesirable transformation between the layered structure and the rock salt phase, further causing capacity decay and a decrease in voltage [4]. Secondly, the surface nickel becomes a high-valent state with high activity during the charging process, which is prone to side reactions with the electrolyte, resulting in a decrease in capacity and an aggravation of polarization. [5]. Thirdly, the surface alkali content for high-nickel cathode materials is high, and it easily reacts with moisture and carbon dioxide in the air. A high alkaline content can aggravate a side reaction with the electrolyte and seriously affect the electrochemical properties of the high-nickel samples [6].

Intensive investigations have proved that element doping and surface modification are effective ways to solve the mentioned shortcomings of NCM811 [7–10]. Substantial efforts have been made to suppress the phase transition and cation disorder. Element doping with the use of elements such as Al, Mg, Ti, Cr, and Zr has previously been adopted in investigations involving the NCM811 material, which proved that element doping is effective in the alleviation of the cation disorder and in the improvement of cycling stability [11–14]. Surface coating is another effective strategy that can be used to suppress the side reaction with the electrolyte. Various coating layers, including metal fluorides such as  $\text{MgF}_2$  [15],  $\text{AlF}_3$  [16],  $\text{CaF}_2$  [17], and  $\text{LaF}_3$  [18], metal oxides such as  $\text{Y}_2\text{O}_3$  [19],  $\text{Al}_2\text{O}_3$  [20],  $\text{MgO}$  [21], and  $\text{ZrO}_2$  [22], and metal phosphates such as  $\text{Li}(\text{PO}_4)_3$  [23],  $\text{Ni}_3(\text{PO}_4)_2$  [24],  $\text{AlPO}_4$  [25],  $\text{MnPO}_4$  [26], and  $\text{LaPO}_4$  [27] have been reported as suitable coating materials, which can effectively reduce direct contact with electrolytes and improve the long cycling process of the host material [23,24]. Feng et al. [28] elaborately obtained the  $\text{Al}(\text{PO}_3)_3$ - $\text{AlPO}_4$ - $\text{Li}_3\text{PO}_4$ -coated NCM811 sample, and the modified sample demonstrated enhanced electrochemical properties, delivering a capacity retention of 85.4% after 50 cycles, which was much higher than the unmodified sample. In addition, Yue et al. reported that the electrochemical properties of  $\text{Y}(\text{PO}_3)_3$ -coated  $\text{LiNi}_{0.6}\text{Co}_{0.1}\text{Mn}_{0.3}\text{O}_2$  were greatly enhanced and found that the  $\text{Y}(\text{PO}_3)_3$ -modified NCM613 sample presented a higher discharge capacity of 181.3 mAh  $\text{g}^{-1}$  at 1 C under room temperature, and it showed a capacity retention rate of 87.2% after 100 charge–discharge cycles, which was higher than the unmodified sample [29].

Among the coating materials, metal phosphate coatings show a positive effect on the electrochemical performance of NCM materials. In a previous report, the phosphate structural unit had a strong binding force with metal ions, which was able to enhance the thermal stability of the matrix sample [27]. The large tetrahedral  $\text{PO}_4^{3-}$  polyanions showed higher electronegativity than  $\text{O}^{2-}$  anions. The  $\text{PO}_4^{3-}$  polyanion groups were doped into layered cathode materials to minimize local structural changes during charge–discharge cycles, and the cathode material maintained the original layered structure during long cycling [30]. Moreover, metal phosphates such as  $\text{AlPO}_4$  showed strong P=O bonds and good ionic conductivity, which could facilitate the diffusion of lithium ions [27].

Coating methods are divided into wet coating and dry coating. In recent reports, wet coating with the NCM cathode material has been the main method of choice [26,31]. Gao et al. adopted a wet grinding procedure to treat a mixture of NCM613 using  $\text{NaH}_2\text{PO}_2$  as the phosphorus precursor [31]. In the work of Chen et al., continuous nanocoating of NCM was successfully realized using a simple wet chemical method with  $\text{NH}_4\text{H}_2\text{PO}_4$  as the phosphorus precursor [26]. Coatings obtained via the wet method are continuous and uniform, however the preparation process is complex, the raw material is expensive, and the preparation process produces waste liquid, so it is difficult to achieve mass production via wet coating. Dry coating is a better choice to achieve coating materials on a matrix surface due to the price advantage, the simple process, and easy industrialization. Lee et al. studied a  $\text{Li}(\text{Ni}_{0.8}\text{Co}_{0.15}\text{Al}_{0.05})\text{O}_2$  sample after  $\text{Ni}_3(\text{PO}_4)_2$  coating via the ball milling method, which showed improved cycling performance at 55 °C [24]. Similarly, a bio-waste-derived, CaO-coated NCM 811 sample was obtained via the dry method, which demonstrated improved reversibility and retention [32]. However, compared with the modified product obtained via the wet coating method, the electrochemical performances of the dry-coated

cathode samples were still lower in comparison. Hence, it is necessary to explore suitable coating compositions and optimal coating processes.

In this study, coating using metal phosphates was investigated as a coating material utilizing  $\text{Al}(\text{PO}_3)_3$  as the precursor of the cladding layer via the dry method of ball milling, followed by the calcination process (400 °C, 500 °C, and 600 °C). We used  $\text{Al}(\text{PO}_3)_3$  as the coating precursor due to the cost advantage of the raw material, the high structural stability, and the easy combination with the residual alkali on the matrix material. The effects of the  $\text{Al}(\text{PO}_3)_3$  calcination temperature on the microstructures, electrochemical performance, and electrochemical boosting mechanism of the NCM811 sample were systematically studied. The  $\text{Al}(\text{PO}_3)_3$ -modified NCM811 material demonstrated superior electrochemical performance, especially at the heated temperature of 500 °C.

## 2. Materials and Methods

### 2.1. Material Preparation

NCM811 powders were purchased from Dongguan East sunshine Scientific Research development Co. LTD, Dongguan, China and nano-scale  $\text{Al}(\text{PO}_3)_3$  powders were purchased from Shanghai Pacific Technology Co., LTD (Shanghai, China). The matrix materials and precursors were obtained directly from the market with no additional pre-treatment. To prepare the  $\text{Al}(\text{PO}_3)_3$ -modified NCM811 sample, 0.4 g of the  $\text{Al}(\text{PO}_3)_3$  sample was mixed with 20 g of NCM811 powders via dry ball milling with a milling speed of 100 rpm for 10 h, and the  $\text{Al}(\text{PO}_3)_3$ -modified powder was annealed for 5 h in air flow at temperatures of 400 °C, 500 °C, and 600 °C. The schematic diagram of the preparation process for  $\text{Al}(\text{PO}_3)_3$ -modified samples is displayed in Figure 1a. The samples heated at 400 °C, 500 °C, and 600 °C are marked as NCM@ALP400, NCM@ALP500, and NCM@ALP600, respectively. Feng et al. have investigated the effect of  $\text{Al}(\text{PO}_3)_3$  coating on the electrochemical performance of NCM811 material with various coating amounts of 1, 2 and 3 wt.% and found that the  $\text{Al}(\text{PO}_3)_3$  coated sample with 2 wt.% amount showed better electrochemical performance [28].

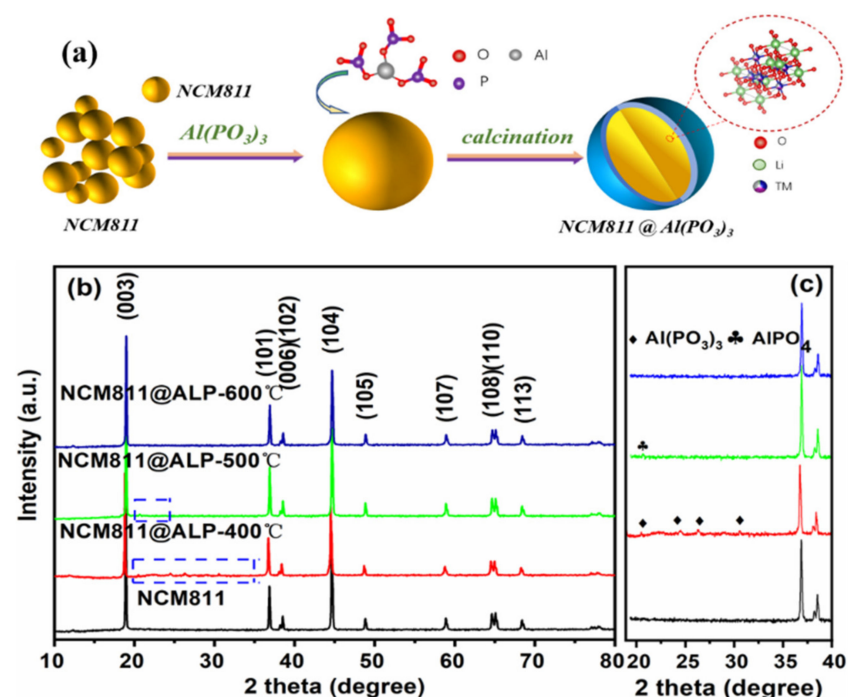


**Figure 1.** (a) The schematic diagram of the preparation process for NCM@ $\text{Al}(\text{PO}_3)_3$ . (b) XRD patterns of pure NCM811 and  $\text{Al}(\text{PO}_3)_3$ -modified NCM811 materials. (c) Zoomed-in XRD patterns of pure NCM811 and modified NCM811 materials.

## 2.2. Material Characterizations

X-ray diffraction (XRD) examinations were conducted on the NCM811 sample and Al(PO<sub>3</sub>)<sub>3</sub>-modified NCM811 samples for phase analysis by using the X'Pert-PRO instrument (Cu-K $\alpha$  radiation) in the scanning range of 10–80°. The cell parameters of the samples were obtained utilizing the JADE software (Jade 6), shown in Table 1. Additionally, XRD patterns were obtained for the electrodes after cycling to analyze the phase change of the samples. To analyze the morphology and the chemical composition of the bare and modified NCM811 samples, scanning electronic microscopy (SEM, Quanta 450 FEG, FEI, Hillsboro, OR, USA) was conducted, combined with energy-dispersive X-ray detection (EDX, Oxford, UK). To inspect the structural features of the original and modified samples, high-resolution transmission electron microscopy (HRTEM, FEI, Hillsboro, OR, USA) and transmission electron microscopy (TEM, FEI, Hillsboro, OR, USA) examinations were conducted using a Talos F200X instrument. The samples were tested using X-ray photoelectron spectroscopy (XPS, ESCALAB 250xi, Waltham, MA, USA) to analyze the surface valence change of the sample surface.

**Table 1.** Lattice parameters of bare and Al(PO<sub>3</sub>)<sub>3</sub>-coated LiNi<sub>0.8</sub>Co<sub>0.1</sub>Mn<sub>0.1</sub>O<sub>2</sub> samples.

Samples	<i>a</i> (Å)	<i>c</i> (Å)	<i>c/a</i>	<i>I</i> (003)/ <i>I</i> (104)
NCM811	2.863	14.098	4.924	1.508
NCM811@ALP400	2.859	14.155	4.951	1.396
NCM811@ALP500	2.861	14.091	4.925	1.549
NCM811@ALP600	2.858	14.107	4.936	1.378

## 2.3. Electrochemical Measurement

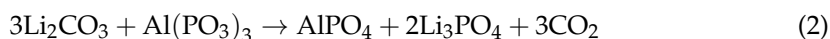
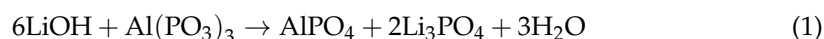
The electrode slurry was dispersed in N-methyl-2-pyrrolidinone by mixing the cathode material, polyvinylidene fluoride, and acetylene black with a mass ratio of 8:1:1. The slurry was spread on Al foil uniformly and was heated at 120 °C for 12 h via vacuum drying, and it was then rolled and punched into disks. The mass load of the electroactive material for each disk was about 2–2.5 mg cm<sup>−2</sup>. The CR2032-type half-coin cells were assembled with the prepared electrode as the cathode, Celgard 2500 as the separator, and lithium metal as the anode. The electrolyte was added into the coin cells with the formula of 1 M LiPF<sub>6</sub> in an EMC:DMC:EC = 1:1:1 volume ratio. Electrochemical performances of the samples were conducted on a Land CT2001A battery test system (1 C = 200 mA g<sup>−1</sup>) in the voltage range of 2.8–4.3 V (vs. Li/Li<sup>+</sup>) at 30 °C and 60 °C. The cyclic voltammetry (CV) curves with the scan range of 2.8–4.5 V and the scan rate of 0.1 mV s<sup>−1</sup> in the first three cycles and the electrochemical impedance spectroscopy (EIS) curves (frequency range, 0.01 Hz to 100 kHz) after 200 cycles were conducted using the electrochemical station (CHI660C, Shanghai, China) to evaluate the electrode reaction process of the NCM811 sample and Al(PO<sub>3</sub>)<sub>3</sub>-modified NCM811 samples.

## 3. Results

The XRD patterns and the enlarged patterns of pure NCM811 and Al(PO<sub>3</sub>)<sub>3</sub>-modified NCM811 are displayed in Figure 1b,c. The lattice parameters of the bare and Al(PO<sub>3</sub>)<sub>3</sub>-modified NCM811 samples are shown in Table 1. The main XRD peaks for the pure NCM811 and the modified materials exhibited the NaFeO<sub>2</sub>-type, hexagonal-layered structure belonging to the R3m space group, which corresponded well with the PDF card #87-1562. The (108)/(110) and (006)/(102) peaks showed obvious cleavage, implying that pure NCM811 and Al(PO<sub>3</sub>)<sub>3</sub>-modified NCM811 maintained a well-developed layered structure [33]. The XRD pattern of NCM811 before and after ball milling is shown in the supporting information of Figure S1. The XRD pattern remains the same before milling and after milling, indicating that ball milling does not affect the purity of the material. Shown in Table 1, the intensity ratios of I(003)/I(004) for all the samples were 1.508, 1.396, 1.549, and 1.378, which are much higher than 1.20, confirming a well-ordered layer structure with low cation

mixing [34]. If the value of  $I(003/004)$  is less than 1.2 in the XRD pattern, this usually indicates the cation mixing appearance as a result of the similar radii of  $\text{Ni}^{2+}$  (0.69 Å) and  $\text{Li}^+$  (0.76 Å) [35]. The results indicate that  $\text{Al}(\text{PO}_3)_3$  modification did not change the main phase structure of the NCM811 material.

To analyze the tiny changes of the phase structure, the zoomed-in XRD patterns are shown in Figure 1c. It is worth noting that the diffraction peaks of  $\text{Al}(\text{PO}_3)_3$  (PDF card of #13-0264) impurity appeared when heated to 400 °C. When heated to 500 °C, the diffraction peaks of  $\text{Al}(\text{PO}_3)_3$  disappeared, and the minor diffraction peaks of  $\text{AlPO}_4$  appeared (PDF card of #47-0168), which implies that the  $\text{Al}(\text{PO}_3)_3$  precursor probably reacted with the lithium-containing compounds on the surface of NCM811 to form  $\text{AlPO}_4$ . According to the previous study [28,29],  $\text{Al}(\text{PO}_3)_3$  reacted with residual lithium on the NCM811 surface, and the probable reactions are listed as Equations (1) and (2). However, the diffraction peaks of  $\text{Li}_3\text{PO}_4$  were not detected in the XRD pattern, which may be due to the low content of  $\text{Li}_3\text{PO}_4$  on the sample surface. The diffraction peaks of  $\text{AlPO}_4$  disappeared at 600 °C, which may be related with the small amount of  $\text{AlPO}_4$  that diffused from the surface into the bulk, accelerated by the increased temperature.



SEM images are shown in Figure 2a–d to observe the coating layer on the original NCM811 surface. It can be seen from Figure 2a–d that samples showed a similar spherical appearance with diameter sizes of 10–20 µm. Regular quasi-spherical particles were composed of small, packed primary particles with particle sizes of 300–500 nm. All of the samples with spherical morphology aided tight packing between the active material and acetylene black, and this could improve the tap density of lithium-ion batteries. Meanwhile, a spherical appearance was beneficial to electrode processing due to the high ductility and low friction. Enlarged SEM images are shown in Figure 2a1–d1. The original NCM811 sample presented a relatively smooth surface, while  $\text{Al}(\text{PO}_3)_3$ -coated NCM811 samples heated to 400 °C and 500 °C displayed rough surfaces with a few fragments and folds. With regard to the bare particles of NCM811, there were gaps between the primary particles, while the gaps between the primary particles almost disappeared for the modified samples, indicating that the primary particles became compact and dense after modification. The disappearing gaps may be ascribed to the formation of the  $\text{Al}(\text{PO}_3)_3$ -based coating distributed in the voids, which was beneficial in reducing the corrosion of the active material by the electrolyte, further restraining the detrimental reactions [36].

Notably, the sample surface of the  $\text{Al}(\text{PO}_3)_3$ -coated NCM811 heated to 600 °C became as smooth as the bare sample, which may be due to the  $\text{Al}(\text{PO}_3)_3$  coating diffusing into the inner grain boundary among the primary particles. To further study the elemental distribution of the coating, EDS testing was conducted on the surface of NCM@ALP500, as shown in Figure 2e. As can be seen, Ni, Co, and Mn elements were clearly observed as the major components of NCM811. In addition, P and Al were distributed in the NCM@ALP500 sample, which confirms that NCM811 was successfully coated with the  $\text{Al}(\text{PO}_3)_3$  coating. It is worth mentioning that a clear distribution of Al was observed around the spherical particles as the test particles were stuck to the aluminum foil.

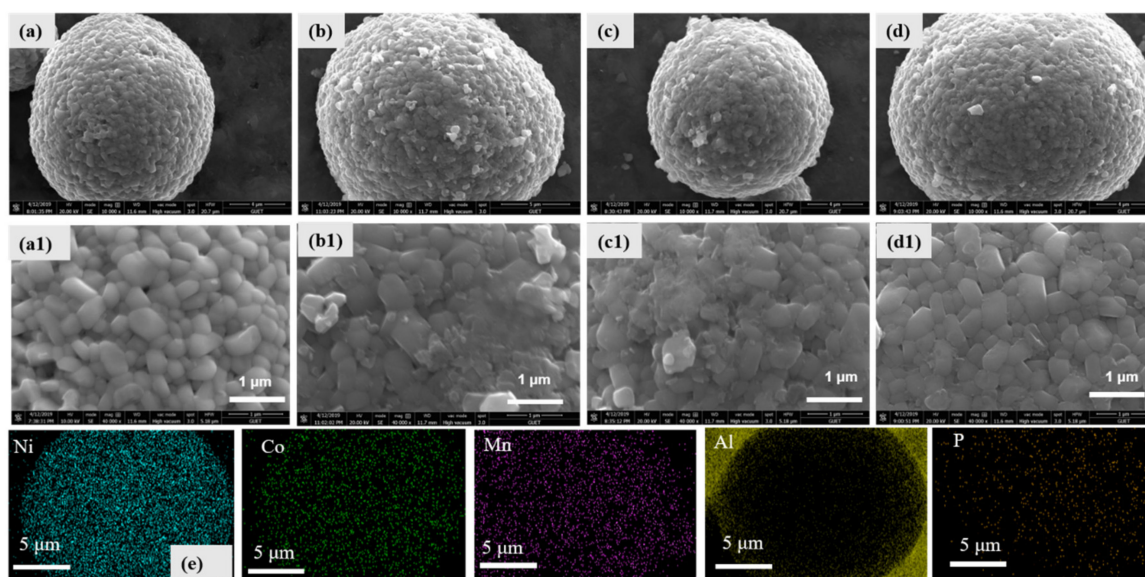


**Figure 2.** SEM images of NCM811 and  $\text{Al}(\text{PO}_3)_3$ -modified NCM811 materials, (a) bare NCM811, (b) NCM811@ALP400, (c) NCM811@ALP500, (d) NCM811@ALP600, (a1–d1) the magnified images of (a–d), (e) EDS mappings of NCM811@ALP500.

HRTEM and TEM measurements were conducted in order to analyze the microstructures of the NCM811 and NCM@ALP500 sample, as shown in Figure 3. As shown in Figure 3a,b, the NCM811 sample had a bare surface with clear lattice fringes of 0.472 nm, 0.237 nm, 0.206 nm, and 0.243 nm, which agreed with the (003), (006), (104), and (101) planes of NCM811 [37]. The corresponding FFT patterns of bare NCM811 are shown in Figure 3b1,b2, indicating a well-ordered layered phase with the  $R\bar{3}m$  space group with no impurity phase. The TEM and HRTEM images of Figure 3c,d clearly show the coating thickness and the lattice fringe of the coating material NCM@ALP500. As seen in Figure 3c, the cladding layer was continuous and tightly combined with the substrate of NCM811, indicating that the coating structure and the host structure possessed good structural compatibility, which is crucial to enhance the long cycling stability of the NCM cathode [38,39]. Nevertheless, the thickness of the coating layer was not very uniform with the thickness range of 10–20 nm, which may be related to the dry-coating process via the ball milling method. As seen from the HRTEM image in Figure 3c,d, the distinct lattice fringe on the coated layer was 0.211 nm, which agreed well with the (117) interplanar spacing of  $\text{AlPO}_4$ , corresponding well with results in the literature [40]. Combined with the XRD, SEM, and TEM results, it can be concluded that the  $\text{AlPO}_4$  coating was successfully attached to the NCM811 substrate for the NCM@ALP500 sample, although the  $\text{AlPO}_4$  coating was low in content, inferred from the XRD pattern.

The surface chemical properties of bare NCM811 and NCM811@ALP500 samples were analyzed by using XPS measurements, displayed in Figure 4a–f. As seen in Figure 4a, the binding energy peaks of the original sample and  $\text{Al}(\text{PO}_3)_3$ -modified sample were located at  $\sim 872.8$  eV ( $\text{Ni } 2p_{1/2}$ ) and  $\sim 855.4$  eV ( $\text{Ni } 2p_{3/2}$ ), corresponding the coexistence of bivalent Ni and trivalent Ni [41]. As seen in Figure 4b, two binding energy peaks for the Co 2p spectra were displayed at 779.7 eV ( $\text{Co } 2p_{3/2}$ ) and 794.5 eV ( $\text{Co } 2p_{1/2}$ ), indicating that Co was mostly presented as a trivalent state in the bare sample and  $\text{Al}(\text{PO}_3)_3$ -modified sample [42]. In Figure 4c, two binding energy peaks for the Mn 2p spectra are displayed at 653.9 eV ( $\text{Mn } 2p_{1/2}$ ) and 641.7 eV ( $\text{Mn } 2p_{3/2}$ ), implying that Mn was mostly tetravalent in the samples [43]. Through the above analysis, it can be seen the  $\text{Al}(\text{PO}_3)_3$  coating and heat treatment had little effect on the valence state of the original NCM sample. In addition, the Al XPS spectrum displayed in Figure 4d was only found for the NCM811@ALP500 sample, which is ascribed to the existence of the  $\text{AlPO}_4$  coating [28]. Meanwhile, the P2p XPS spectrum with one binding energy peak at 133.5 eV was only detected for the

NCM811@ALP500 sample, belonging to the tetrahedral  $\text{PO}_4$  [44], which indicates the existence of  $\text{PO}_4^{3-}$  in the coating layer. XPS spectra of Al and P further indicate that the  $\text{AlPO}_4$  coating layer was successfully coated on the NCM811@ALP500 surface.

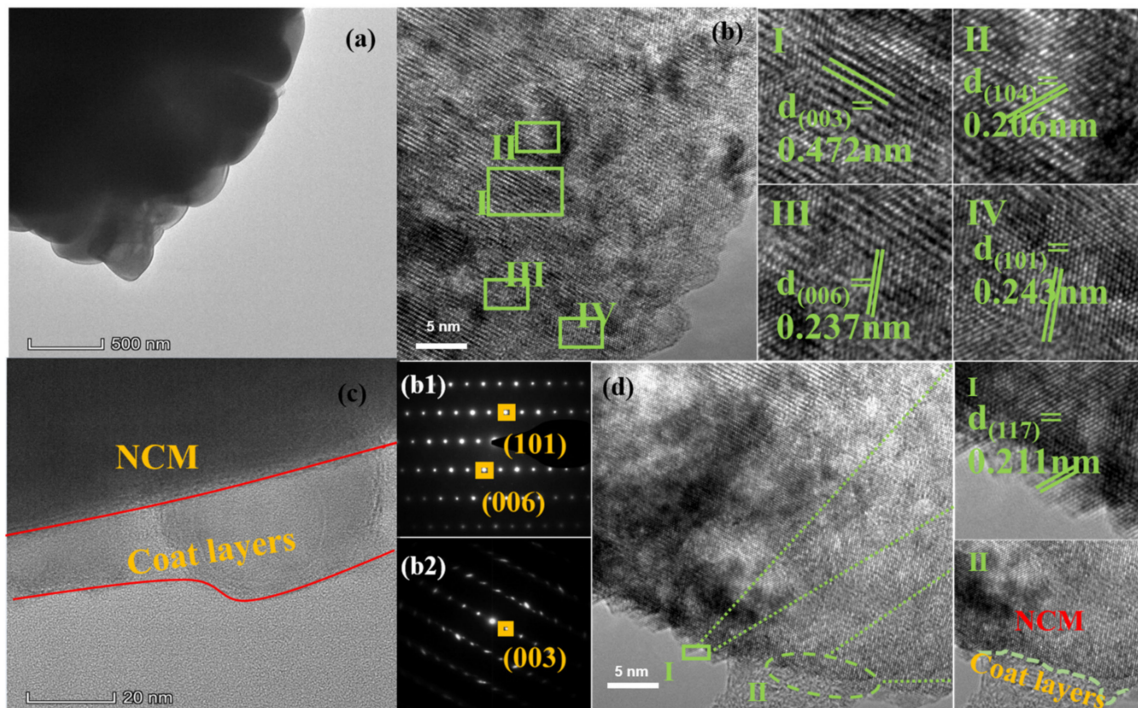


**Figure 3.** (a) TEM images of as-prepared NCM811 cathodes and the corresponding HRTEM images of NCM811 shown as (I–IV). (b,c) show the fast Fourier transform (FFT) patterns of NCM811. (d) TEM images of NCM811@ALP500 and the corresponding HRTEM images, shown as (I,II). (b1) is area (IV); (b2) is area (I).

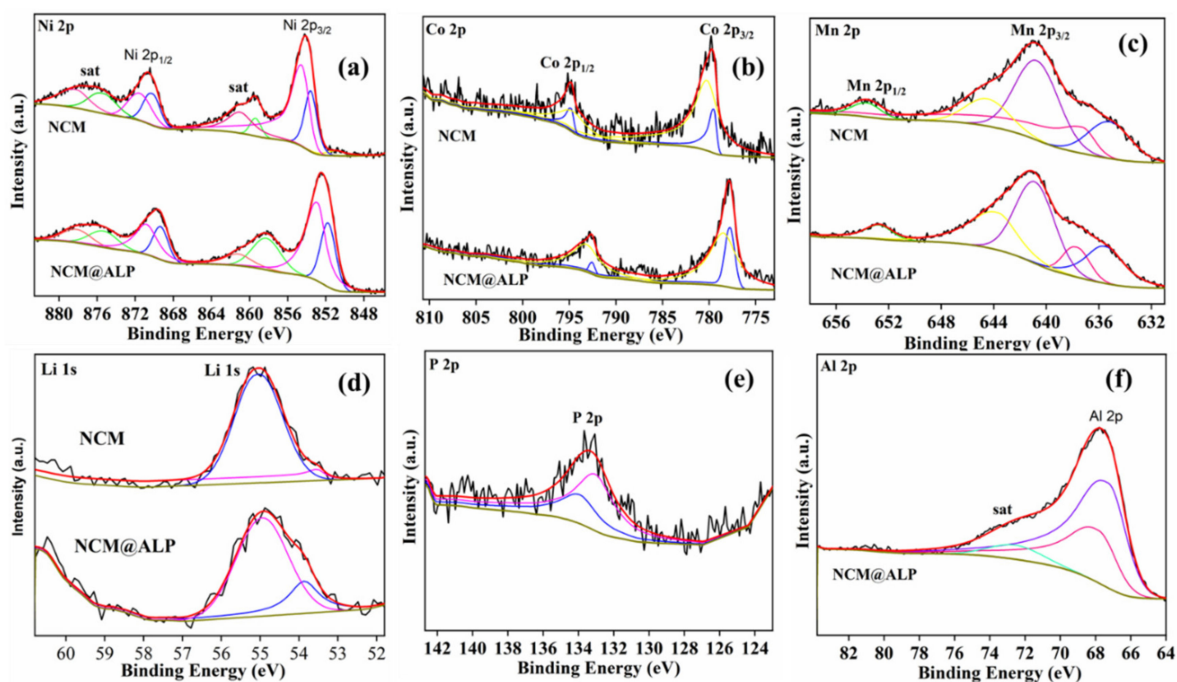


**Figure 4.** XPS spectra for NCM811 and NCM811@ALP500, (a–d) XPS spectra of Ni, Co, Mn, and Li for NCM811 and NCM811@ALP 500 samples, (e–f) XPS spectra of P and Al elements for NCM811@ALP500.

The initial galvanostatic discharging data of the unmodified NCM811, NCM811@ALP400, NCM811@ALP500, and NCM811@600 electrodes at 0.2 C ( $1\text{ C} = 200\text{ mA g}^{-1}$ ) at  $30\text{ }^{\circ}\text{C}$  are shown in Figure 5a. The coated samples exhibited similar discharge platforms compared with the bare NCM811, indicating that the  $\text{Al}(\text{PO}_3)_3$  coating did not alter the charging and discharging reaction. However, the initial discharge capacities showed a slight downward trend after  $\text{Al}(\text{PO}_3)_3$  coating. The pristine NCM811 sample demonstrated the discharge capacity of  $200.4\text{ mAh g}^{-1}$ , while the modified samples exhibited the discharge capacities of  $185.6\text{ mAh g}^{-1}$ ,  $196.5\text{ mAh g}^{-1}$ , and  $197.1\text{ mAh g}^{-1}$  for ALP400, ALP500, and ALP 600, respectively. The decrease in discharge capacity can be attributed to the fact that the  $\text{Al}(\text{PO}_3)_3/\text{AlPO}_4$  coating layer was inactive and did not contribute capacity. The cycling performances of the samples at 1 C (activated after five cycles at 0.2 C) are demonstrated in Figure 5b in the voltage range of 2.7–4.3 V, and the corresponding electrochemical parameters are listed in Table 2. The modified NCM electrodes showed remarkable enhancement in the cyclability after  $\text{Al}(\text{PO}_3)_3$  modification, especially for the NCM811@ALP500 sample. Under a charge–discharge current of 1 C, the capacity of the bare NCM decreased from  $178.3\text{ mAh g}^{-1}$  to  $122.5\text{ mAh g}^{-1}$  after 200 charging–discharging cycles with a capacity retention ratio of 68.70%. The capacity retention increased to 90.28% (ALP400), 93.88% (ALP500), and 86.49% (ALP600) after  $\text{Al}(\text{PO}_3)_3$  modification. It was found that the NCM811@ALP500 sample demonstrated a superior discharge capacity of  $167.2\text{ mAh g}^{-1}$  even after 200 charge–discharge cycles. The significantly improved capacity retention of the NCM811@ALP500 electrode can be attributed to the  $\text{AlPO}_4$  coating layer, which may have inhibited harmful reactions at the interface between the electrolytes and active materials and improved the stability of the crystal structure, thereby enhancing the cycle stability of the materials [45]. This deduction was consistent with the XRD pattern (Figure 1b) that showed the NCM811@ALP500 sample demonstrated the lowest  $\text{Li}^+/\text{Ni}^{2+}$  mixing rate with the higher  $I(003)/I(104)$  value of 1.549. For the ALP400 sample, the capacity retention was basically satisfactory, however the initial capacity was low ( $162.5\text{ mAh g}^{-1}$ ), which was due to the fact that the formed  $\text{Al}(\text{PO}_3)_3$  coating at  $400\text{ }^{\circ}\text{C}$  was thick and uneven. For the ALP600 sample, the capacity retention declined, which could be attributed to the fact that the coating was applied in too low a content to resist the electrolyte attack.

In order to evaluate the electrochemical properties of the samples at elevated temperature, the cycling performances at  $60\text{ }^{\circ}\text{C}$  of the samples at 1 C are displayed in Figure 5c. Compared with the bare sample with the capacity retention of 57.91%, the capacity retentions of the modified samples were 81.01% (ALP400), 83.99% (ALP500), and 78.89% (ALP600) after 55 cycles. At the higher temperature of  $60\text{ }^{\circ}\text{C}$ , the capacity retention ratio decayed faster than that at  $30\text{ }^{\circ}\text{C}$ , however the capacity retention ratio of the sample was significantly improved after  $\text{Al}(\text{PO}_3)_3$  modification, indicating that the  $\text{Al}(\text{PO}_3)_3/\text{AlPO}_4$  coating on the NCM surface aided the inhibition of direct contact with the electrolyte, further suppressing HF attack and oxygen release. Moreover, the  $\text{Al}(\text{PO}_3)_3/\text{AlPO}_4$  surface coating was extremely helpful in improving the structure stability and electrochemical stability of the material, especially at higher temperatures. The rate properties of NCM811 and  $\text{Al}(\text{PO}_3)_3$ -coated samples were tested in 2.8–4.3 V at  $30\text{ }^{\circ}\text{C}$ , as shown in Figure 5d. At a lower current density of 0.2 C–1 C, the discharge capacities of the ALP400, ALP500, and ALP600 samples were close to the original sample or slightly lower than that of the original sample. At a larger current density of 5 C, the discharge capacity of the ALP500 sample was significantly improved compared to the original sample. According to Equation (1), when  $\text{AlPO}_4$  is generated,  $\text{Li}_3\text{PO}_4$  is generated at the same time. According to the XRD and TEM results,  $\text{AlPO}_4$  was indeed formed on the NCM 811 surface after being heated to  $500\text{ }^{\circ}\text{C}$ . However,  $\text{Li}_3\text{PO}_4$  was not observed, which may have been due to the low content. It was previously reported that  $\text{Li}_3\text{PO}_4$  has good  $\text{Li}^+$  transfer characteristics, and at the same time,  $\text{Li}_3\text{PO}_4$  consumes residual lithium compounds on the surface of a sample that is not conducive to  $\text{Li}^+$  conduction [46], so the rate performance of the ALP500 sample was improved.

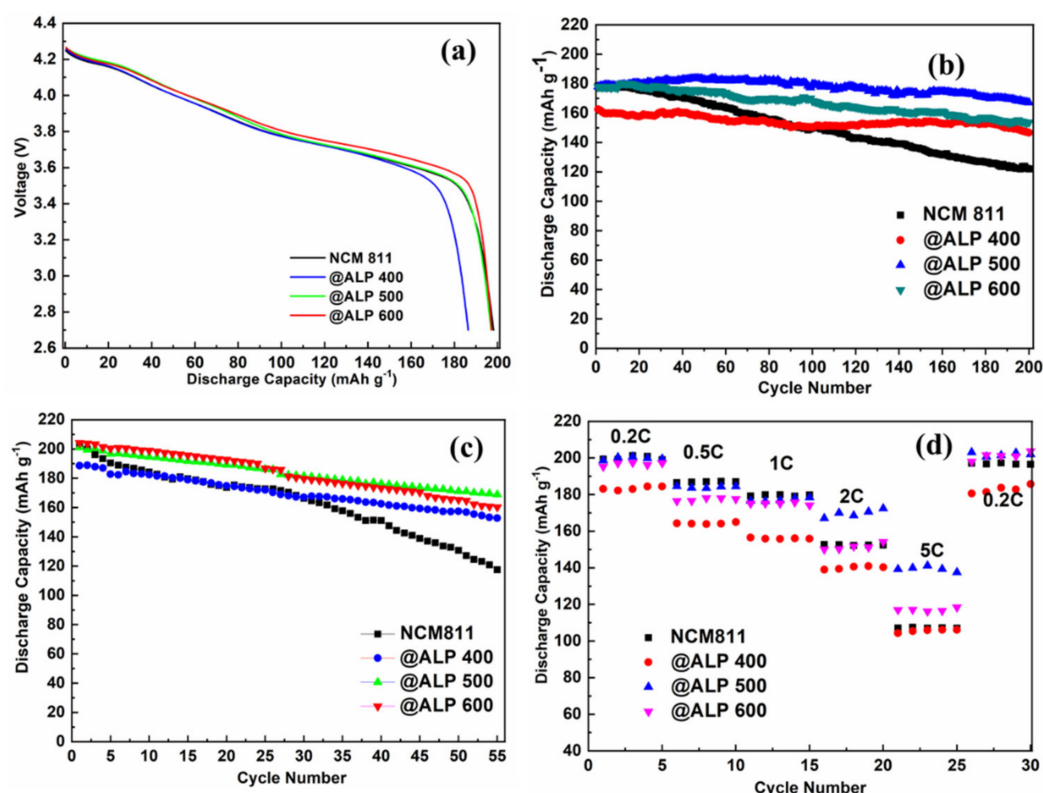


**Figure 5.** (a) Initial discharge curves at 0.2 C in the range of 2.7–4.3 V at 30 °C for bare NCM811 and NCM811@ALP samples. (b) Cycle performances for bare NCM811 and NCM811@ALP samples at 1 C in the range of 2.7–4.3 V at 30 °C. (c) Cycle performances for bare NCM811 and NCM811@ALP samples at 1 C in the range of 2.7–4.3 V at 60 °C. (d) Rate capacities from 0.2 C to 5 C for bare NCM811 and NCM811@ALP samples in the range of 2.7–4.3 V at 30 °C.

**Table 2.** Electrochemical performance of the pristine and Al(PO<sub>3</sub>)<sub>3</sub>-coated LiNi<sub>0.8</sub>Co<sub>0.1</sub>Mn<sub>0.1</sub>O<sub>2</sub> samples.

Systems	Initial Discharge Capacity (mAh g <sup>-1</sup> , 0.2 C)	1st Discharge Capacity (mAh g <sup>-1</sup> , 1 C)	200th Discharge Capacity (mAh g <sup>-1</sup> , 1 C)	Capacity Retention (%)
Original	200.4	178.3	122.5	68.70
NCM811@ALP400	185.6	162.5	146.7	90.28
NCM811@ALP500	196.5	178.1	167.2	93.88
NCM811@ALP600	197.1	177.6	153.6	86.49

The cyclic voltammetry (CV) curves were conducted on bare NCM811 and the ALP500 sample to further study the electrochemical performance, shown in Figure 6a,b. The CV curves of the bare NCM811 and NCM811@ALP500 sample exhibited a similar trend, implying that the Al(PO<sub>3</sub>)<sub>3</sub> coating did not alter the electrochemical reaction. As can be seen in Figure 6a,b, a couple of redox peaks occurred that corresponded to the transition of Ni<sup>2+</sup> to Ni<sup>4+</sup> during the delithiation/intercalation process in the range of 2.8–4.3 V [29]. The difference between the oxidation potential and reduction potential (E<sub>oxidation</sub>-E<sub>reduction</sub>) is usually adopted to evaluate the electrochemical polarization reaction [47]. The difference in ΔE was small, indicating that polarization was not severe. From the first CV curves, the ΔV value of NCM811 was 0.66 V, which was higher than that of the ALP500 sample (0.51 V). The shrinking of the ALP500 sample confirmed that the AlPO<sub>4</sub> coating decreased the polarization phenomenon of NCM811, which was beneficial for the electrochemical reactions under high current density, consistent with the high rate performance. In the second cycle, the redox peaks of NCM811 were located at 3.92 V/3.60 V and 4.30 V/4.09 V, corresponding

to the transition of  $\text{Ni}^{2+}/\text{Ni}^{3+}$  and  $\text{Ni}^{3+}/\text{Ni}^{4+}$ . The redox peaks of the ALP500 sample were located at 3.92 V/3.62 V and 4.29 V/4.10 V. The differences of  $\Delta E$  became smaller during cycling. Moreover, the ALP500 sample exhibited highly overlapping reduction peaks in comparison to bare NCM811 in the first three cycles, revealing that the NCM811@ALP500 sample showed less irreversible capacity, which was conducive to suppressing detrimental reactions in the interface between electrolytes and electrodes. Hence, the NCM811@ALP500 sample demonstrated long-term cycling stability after 200 cycles.

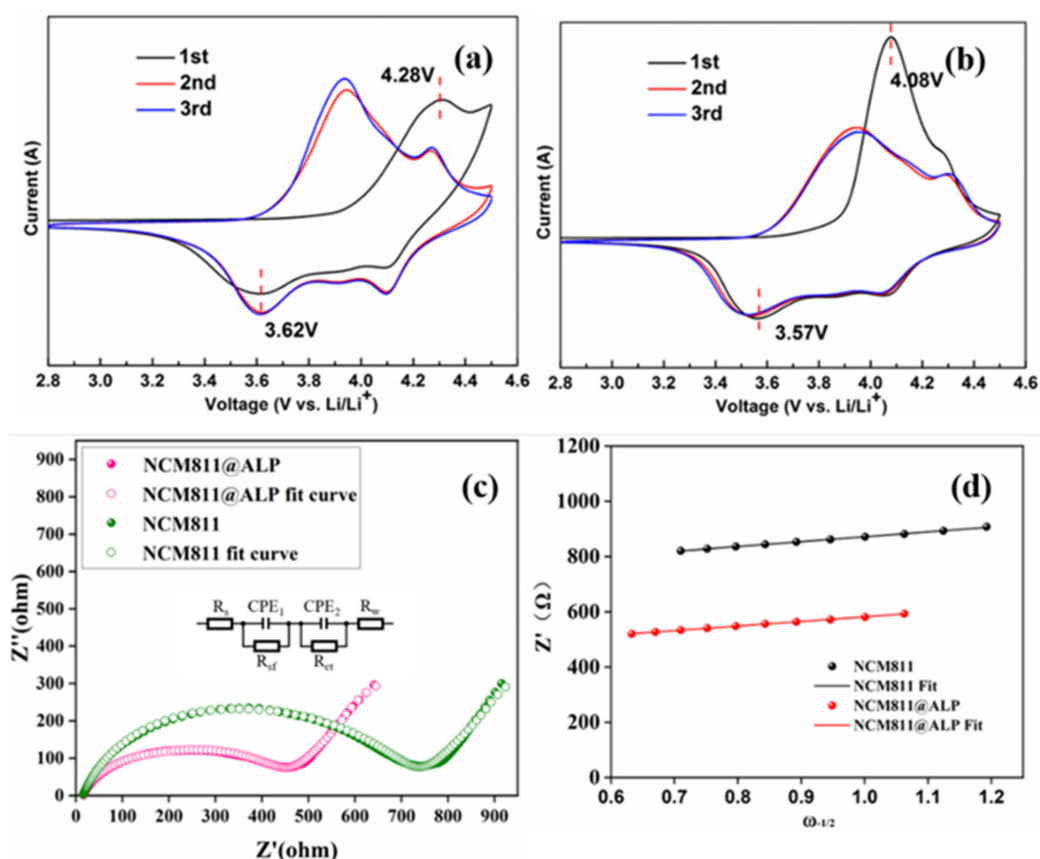


**Figure 6.** (a) CV profiles for NCM811 in the first three cycles. (b) CV profiles for NCM811@ALP 500 in the first three cycles. (c) Nyquist plots and the fitted Nyquist plots with equivalent circuit (insert graph) for NCM811 and NCM811@ALP 500 electrodes after 200 charge–discharge cycles. (d) The relationships between  $Z'$  and  $\omega^{-1/2}$  based on (c).

To explore the electrochemical inner kinetic performances of the improved cycling life after  $\text{Al}(\text{PO}_3)_3$  modification, the EIS of the pristine NCM811 and NCM811@ALP500 electrodes were conducted after 200 charge–discharge cycles. Figure 6c demonstrates the Nyquist plots, including a semicircle at high frequency and a quasi-straight line at low frequency. Usually, the quasi-straight line stands for the Warburg impedance ( $Z_w$ ), corresponding well with lithium-ion diffusion in the matrix NCM electrode [48]. By fitting the EIS curves, the equivalent circuit is shown in Figure 6c (embedded part). To analyze the fitting results of the contribution of  $CPE_1$  and  $CPE_2$  and the goodness of fitting factor, the fitting parameters are provided in the supporting information (Figure S2). The equivalent circuit consists of  $R_e$ ,  $R_{sf}$ , and  $R_{ct}$ , which represent the internal resistance, surface film resistance, and charge transfer resistance, respectively [49,50]. The fitted values of  $R_e$ ,  $R_{sf}$ , and  $R_{ct}$  are shown in Table 3. Obviously,  $R_{sf}$  was much smaller than  $R_{ct}$  for both NCM811 and the coated sample, indicating that  $R_{ct}$  was the major factor affecting the electrochemical reaction. It is noted that the  $R_{ct}$  value of the NCM811@ALP500 electrode was comparatively smaller compared to the original NCM811 after 200 cycles, indicating that optional amount of  $\text{AlPO}_4$  coat layer could decrease the charge transfer resistance after long cycles. These

results further verify our conclusion that the  $\text{AlPO}_4$  coating on the NCM 811 surface can suppress side reactions and enhance the structural stability of the active material.

**Table 3.** The fitted values of  $R_s$ ,  $R_{sf}$ , and  $R_{ct}$  and the calculated values of  $D_{\text{Li}^+}$  of the pristine and  $\text{Al}(\text{PO}_3)_3$ -coated  $\text{LiNi}_{0.8}\text{Co}_{0.1}\text{Mn}_{0.1}\text{O}_2$  samples before and after cycling.

Electrode	$R_s$ ( $\Omega$ )	$R_{sf}$ ( $\Omega$ )	$R_{ct}$ ( $\Omega$ )	$D_{\text{Li}^+}$ ( $\text{cm}^2 \text{s}^{-1}$ )
NCM811	15.9	197.9	720.2	$1.28 \times 10^{-14}$
NCM811@ALP500	16.5	166.9	437.1	$1.44 \times 10^{-14}$

The  $\text{Li}^+$  diffusion coefficients ( $D_{\text{Li}^+}$ ) were calculated using Equation (3). In Equation (3), these parameters ( $R$ ,  $T$ ,  $C$ ,  $F$ ,  $A$ , and  $n$ ) were widely reported in the previous literature and were treated with fixed values [49,51]. The  $\sigma$  value played the decisive role, which represents the Warburg coefficient [49]. The  $\sigma$  value could be obtained from the slope of the linear fitting of resistance ( $Z'$ ) vs. the reciprocal square roots of the frequency ( $\omega^{-1/2}$ ) [51]. The fitted line of  $Z'$  vs.  $\omega^{-1/2}$  is displayed in Figure 6d. The obtained  $D_{\text{Li}^+}$  is listed in Table 3 according to Equation (3).

$$D_{\text{Li}^+} = \frac{R^2 T^2}{2A^2 n^4 F^4 C^2 \sigma^2} \quad (3)$$

For the pristine NCM811 electrode, the calculated  $D_{\text{Li}^+}$  value was  $1.28 \times 10^{-14} \text{ cm}^2 \text{ s}^{-1}$  after 200 cycles, while the  $D_{\text{Li}^+}$  value increased to  $1.44 \times 10^{-14} \text{ cm}^2 \text{ s}^{-1}$  for NCM811@ALP500, indicating that the  $\text{AlPO}_4$  coating aided the suppression of side effects and was beneficial for the electron transfer during charge–discharge, subsequently reducing the interfacial resistance and enhancing the electrode kinetics, consistent with the electrochemical performance after cycling in Figure 5b.

To explore the effect of  $\text{Al}(\text{PO}_3)_3$  modification on the structure of  $\text{LiNi}_{0.8}\text{Co}_{0.1}\text{Mn}_{0.1}\text{O}_2$  after 200 cycles, XRD tests were utilized for the bare NCM811 and NCM811@ALP500, as shown in Figure 7. In general, NCM811 and NCM811@ALP500 cathodes preserved the original layered structure. Compared with Figure 1b, the intensities of all diffraction peaks for the bare NCM811 and NCM811@ALP500 became weaker during 200 charge–discharge cycles, which indicates that the main phase structures suffered from a certain degree of damage. For the bare NCM811 cathodes, the peak intensity ratio of  $I(003)/I(104)$  planes decreased to 0.81, which was much lower than 1.2, after 200 cycles, indicating severe Li/Ni cation mixing. The peak intensity ratio of  $I(003)/I(104)$  planes remained 1.41 for the NCM811@ALP500 cathode, with lower Li/Ni cation mixing after cycling, ensuring the smooth transfer of lithium ions. It is worth noting that the splitting peaks of  $(006)/(102)$  could still be clearly preserved for NCM811@ALP500 and NCM811@ALP600, while the splitting peaks of  $(006)/(102)$  were almost invisible for bare NCM811. These findings further confirm that  $\text{Al}(\text{PO}_3)_3$  modification with suitable heat treatment is helpful in stabilizing the layered structure of the NCM811 electrode during a long cycle. The XRD results correspond well with the electrochemical properties in Figure 5b, which shows NCM811@ALP500 demonstrates good capacity retention due to the modified structure after  $\text{AlPO}_4$  coating.

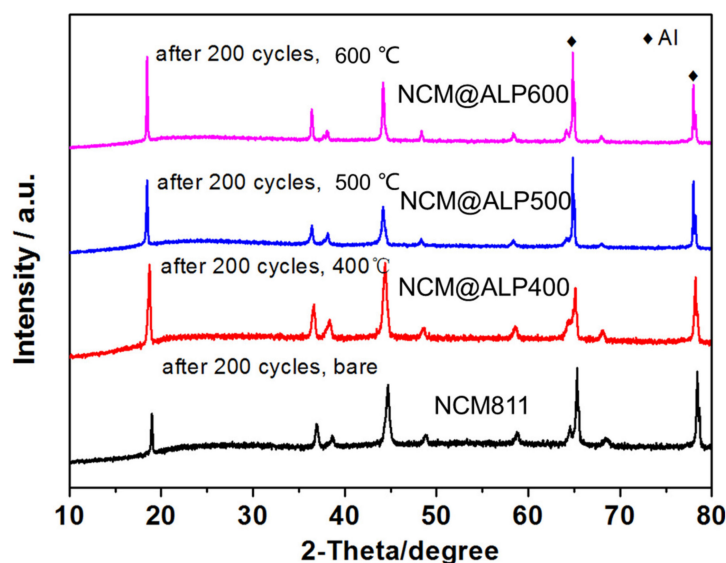


**Figure 7.** XRD patterns of bare NCM811 and NCM811@ALP samples after 200 charge–discharge cycles.

#### 4. Conclusions

To enhance the electrochemical properties of NCM811 and inhibit the interfacial detrimental reactions in contact with the electrolyte, NCM811 was modified with an  $\text{Al}(\text{PO}_3)_3$  precursor via dry ball milling followed by heat treatment. Combined with the XRD, SEM, and XPS characterization, the  $\text{Al}(\text{PO}_3)_3$  coating layer was obtained on the sample surface at the lower sintering temperature of 400 °C, while  $\text{AlPO}_4$  coating was adapted on the NCM811 sample at the higher sintering temperature of 500 °C. The long cycle performance was substantially enhanced after  $\text{Al}(\text{PO}_3)_3$  modification, with a slight decrease in the initial discharge capacity. The NCM811@ALP500 sample maintained a capacity retention of 93.88% after 200 cycles, with an initial discharge capacity of  $178.1 \text{ mAh g}^{-1}$  in 2.7–4.3 V at 1 C at 30 °C, which was much higher than the capacity retention of the bare NCM811 electrode (68.70% with the initial capacity of  $178.3 \text{ mAh g}^{-1}$ ). In addition, NCM811@ALP500 showed a much-improved rate performance compared to the bare NCM811 at 5 C. Confirmed by the EIS analysis, the value of transfer resistance ( $R_{ct}$ ) for the NCM811@ALP500 sample decreased, and the  $D_{\text{Li}^+}$  value increased compared with the bare NCM811 after 200 cycles. It can be concluded that improved electrochemical properties can be achieved via  $\text{Al}(\text{PO}_3)_3$  modification, which can be ascribed to the generated  $\text{AlPO}_4$  coating, inhibiting side reactions and slowing down structural deterioration, further stabilizing the layered structure of NCM811.

**Supplementary Materials:** The following are available online at <https://www.mdpi.com/article/10.3390/coatings12030319/s1>, Figure S1: The XRD pattern of NCM811 before milling and after milling. Figure S2: (a) The fitting details of EIS plot for NCM811; (b) The fitting details of EIS plot for NCM811@ALP.

**Author Contributions:** Conceptualization and Original Draft Preparation, F.W.; Methodology and Software, Y.L. and P.L.; Data Curation, J.D.; Review and Editing, M.-S.B.; Project Administration, Z.W. All authors have read and agreed to the published version of the manuscript.

**Funding:** This work was supported by the Natural Science Foundation of Guangxi Province (2019GXNSFDA245014 and 2019GXNSFBA245055). This work was also funded by the Science and Technology Base and Talent Special Project of Guangxi Province, China (AD19245030 and AD19245162).

**Institutional Review Board Statement:** Not applicable.

**Informed Consent Statement:** Not applicable.

**Data Availability Statement:** Not applicable.

**Conflicts of Interest:** The authors declare no conflict of interest.

## References

1. Ray, A.; Saruhan, B. Application of Ionic Liquids for Batteries and Supercapacitors. *Materials* **2021**, *14*, 2942. [[CrossRef](#)] [[PubMed](#)]
2. Wu, F.; Li, Q.; Chen, L.; Lu, Y.; Su, Y.; Bao, L.; Chen, R.; Chen, S. Use of Ce to reinforce the interface of Ni-rich  $\text{LiNi}_{0.8}\text{Co}_{0.1}\text{Mn}_{0.1}\text{O}_2$  cathode materials for lithium-ion batteries under high operating voltage. *ChemSusChem* **2019**, *12*, 935–943. [[CrossRef](#)]
3. Xu, T.; Li, Y.; Wang, D.; Wu, M.; Pan, D.; Zhao, H.; Bai, Y. Enhanced electrochemical performance of  $\text{LiNi}_{0.5}\text{Mn}_{1.5}\text{O}_4$  cathode material by  $\text{YPO}_4$  surface modification. *ACS Sustain. Chem. Eng.* **2018**, *6*, 5818–5825. [[CrossRef](#)]
4. Dong, M.X.; Wang, Z.X.; Li, H.K.; Guo, H.J.; Li, X.H.; Shih, K.; Wang, J.X. Metallurgy inspired formation of homogeneous  $\text{Al}_2\text{O}_3$  coating layer to improve the electrochemical properties of  $\text{LiNi}_{0.8}\text{Co}_{0.1}\text{Mn}_{0.1}\text{O}_2$  cathode material. *ACS Sustain. Chem. Eng.* **2017**, *5*, 10199–10205. [[CrossRef](#)]
5. Ren, X.G.; Li, Y.J.; Xi, X.M.; Liu, S.W.; Xiong, Y.K.; Zhang, D.W.; Wang, S.; Zheng, J.C. Modification of  $\text{LiNi}_{0.8}\text{Co}_{0.1}\text{Mn}_{0.1}\text{O}_2$  cathode materials from the perspective of chemical stabilization and kinetic hindrance. *J. Power Sources* **2021**, *499*, 229756. [[CrossRef](#)]
6. Marina, A.H.; Ilea, P. Enhancing Lithium Manganese oxide electrochemical behavior by doping and surface modifications. *Coatings* **2021**, *11*, 456. [[CrossRef](#)]
7. Xu, C.; Guan, S.; Li, L.; Sun, C.; An, B.; Geng, X. Electrochemical properties of  $\text{LiNi}_{0.6}\text{Co}_{0.2}\text{Mn}_{0.2}\text{O}_2$  cathode materials prepared with different Ammonia content. *Coatings* **2021**, *11*, 932. [[CrossRef](#)]
8. Susai, F.A.; Kovacheva, D.; Kravchuk, T.; Kauffmann, Y.; Maiti, S.; Chakraborty, A.; Kunnikuruvaan, S.; Talianker, M.; Sclar, H.; Fleger, Y. Studies of Nickel-rich  $\text{LiNi}_{0.85}\text{Co}_{0.10}\text{Mn}_{0.05}\text{O}_2$  cathode materials doped with Molybdenum ions for Lithium-ion batteries. *Materials* **2021**, *14*, 2070. [[CrossRef](#)]
9. Jung, J.S.; Yim, H.; Parmar, N.S.; Lee, J.S.; Choi, J.W. Continuous composition spread and electrochemical studies of low cobalt content  $\text{Li}(\text{Ni},\text{Mn},\text{Co})\text{O}_2$  cathode materials. *Coatings* **2019**, *9*, 366. [[CrossRef](#)]
10. Somo, T.R.; Mabokela, T.E.; Teffu, D.M.; Sekgobela, T.K.; Ramogayana, B.; Hato, M.J.; Modibane, K.D. A Comparative review of metal oxide surface coatings on three families of cathode materials for Lithium-ion batteries. *Coatings* **2021**, *11*, 744. [[CrossRef](#)]
11. Han, B.; Key, B.; Lapidus, S.H.; Garcia, J.C.; Iddir, H.; Vaughney, J.T.; Dogan, F. From coating to dopant: How the transition metal composition affects alumina coatings on Ni-rich cathodes. *ACS Appl. Mater. Interfaces* **2017**, *9*, 41291–41302. [[CrossRef](#)]
12. Tu, J.; Wu, K.; Tang, H.; Zhou, H.; Jiao, S. Mg-Ti co-doping behavior of porous  $\text{LiFePO}_4$  microspheres for high-rate lithium-ion batteries. *J. Mater. Chem.* **2017**, *5*, 17021–17028. [[CrossRef](#)]
13. Zhu, W.; Liu, D.; Trottier, J.; Gagnon, C.; Howe, J.; Mauger, A.; Julien, C.M.; Zaghi, K. In-situ Raman spectroscopic investigation of  $\text{LiMn}_{1.45}\text{Ni}_{0.45}\text{M}_{0.1}\text{O}_4$  ( $M = \text{Cr}, \text{Co}$ ) 5 V cathode materials. *J. Power Sources* **2015**, *298*, 34. [[CrossRef](#)]
14. Schipper, F.; Bouzaglio, H.; Dixit, M.; Erickson, E.M.; Weigel, T.; Talianker, M.; Grinblat, J.; Burstein, L.; Schmidt, M.; Lampert, J.; et al. From surface  $\text{ZrO}_2$  coating to bulk Zr doping by high temperature annealing of Nickel-rich lithiated oxides and their enhanced electrochemical performance in Lithium-ion batteries. *Adv. Energy Mater.* **2017**, *17*, 1682. [[CrossRef](#)]
15. Sun, S.; Wan, N.; Wu, Q.; Zhang, X.; Pan, D.; Bai, Y.; Lu, X. Surface-modified  $\text{Li}[\text{Li}_{0.2}\text{Ni}_{0.17}\text{Co}_{0.07}\text{Mn}_{0.56}]\text{O}_2$  nanoparticles with  $\text{MgF}_2$  as cathode for Li-ion battery. *Solid State Ionics* **2015**, *278*, 85–90. [[CrossRef](#)]
16. Yang, K.; Fan, L.Z.; Guo, J.; Qu, X. Significant improvement of electrochemical properties of  $\text{AlF}_3$ -coated  $\text{LiNi}_{0.5}\text{Co}_{0.2}\text{Mn}_{0.3}\text{O}_2$  cathode materials. *Electrochim. Acta* **2012**, *63*, 363–368. [[CrossRef](#)]
17. Xu, K.; Jie, Z.; Li, R.; Chen, Z.; Wu, S.; Gu, J.; Chen, J. Synthesis and electrochemical properties of  $\text{CaF}_2$ -coated for long-cycling  $\text{Li}[\text{Mn}_{1/3}\text{Co}_{1/3}\text{Ni}_{1/3}]\text{O}_2$  cathode materials. *Electrochim. Acta* **2012**, *60*, 130–133. [[CrossRef](#)]
18. Chen, Q.; Wang, Y.; Zhang, T.; Yin, W.; Yang, J.; Wang, X. Electrochemical performance of  $\text{LaF}_3$ -coated  $\text{LiMn}_2\text{O}_4$  cathode materials for lithium-ion batteries. *Electrochim. Acta* **2012**, *83*, 65–72. [[CrossRef](#)]
19. Wang, Y.Y.; Gao, M.Y.; Liu, S.; Li, G.R.; Gao, X.P. Yttrium surface gradient doping for enhancing structure and thermal stability of high-Ni layered oxide as cathode for Li-ion batteries. *ACS Appl. Mater. Interfaces* **2021**, *13*, 7343–7354. [[CrossRef](#)]
20. Chen, Y.; Zhang, Y.; Wang, F.; Wang, Z.; Zhang, Q. Improve the structure and electrochemical performance of  $\text{LiNi}_{0.6}\text{Co}_{0.2}\text{Mn}_{0.2}\text{O}_2$  cathode material by nano- $\text{Al}_2\text{O}_3$  ultrasonic coating. *J. Alloys Compd.* **2014**, *611*, 135–141. [[CrossRef](#)]
21. Kumar, A.; Nazzario, R.; Torres-Castro, L.; Pena-Duarte, A.; Tomar, M.S. Electrochemical properties of  $\text{MgO}$ -coated  $0.5\text{Li}_2\text{MnO}_3$ - $0.5\text{LiNi}_{0.5}\text{Mn}_{0.5}\text{O}_2$  composite cathode material for lithium ion battery. *Int. J. Hydrog. Energy* **2015**, *40*, 4931–4935. [[CrossRef](#)]
22. Kong, J.Z.; Wang, S.S.; Tai, G.A.; Wang, L.G.; Zhai, H.F.; Wu, D.; Li, A.D.; Li, H. Enhanced electrochemical performance of  $\text{LiNi}_{0.5}\text{Co}_{0.2}\text{Mn}_{0.3}\text{O}_2$  cathode material by ultrathin  $\text{ZrO}_2$  coating. *J. Alloys Compd.* **2016**, *657*, 593–600. [[CrossRef](#)]
23. Tang, Z.F.; Wu, R.; Huang, P.F.; Wang, Q.S.; Chen, C.H. Improving the electrochemical performance of Ni-rich cathode material  $\text{LiNi}_{0.815}\text{Co}_{0.15}\text{Al}_{0.035}\text{O}_2$  by removing the lithium residues and forming  $\text{Li}_3\text{PO}_4$  coating layer. *J. Alloys Compd.* **2017**, *693*, 1157–1163. [[CrossRef](#)]
24. Lee, D.J.; Scrosati, B.; Sun, Y.K.  $\text{Ni}_3(\text{PO}_4)_2$ -coated  $\text{Li}[\text{Ni}_{0.8}\text{Co}_{0.15}\text{Al}_{0.05}]\text{O}_2$  lithium battery electrode with improved cycling performance at  $55^\circ\text{C}$ . *J. Power Sources* **2011**, *196*, 7742–7746. [[CrossRef](#)]
25. Cho, J.; Kim, H.; Park, B. Comparison of overcharge behavior of  $\text{AlPO}_4$ -coated  $\text{LiCoO}_2$  and  $\text{LiNi}_{0.8}\text{Co}_{0.1}\text{Mn}_{0.1}\text{O}_2$  cathode materials in Li-ion cells. *J. Electrochem. Soc.* **2004**, *151*, 1707–1711. [[CrossRef](#)]

26. Chen, Z.; Kim, G.T.; Bresser, D.; Diemant, T.; Asenbauer, J.; Jeong, S.; Copley, M.; Behm, R.J.; Lin, J.; Shen, Z.; et al. MnPO<sub>4</sub>-coated Li(Ni<sub>0.4</sub>Co<sub>0.2</sub>Mn<sub>0.4</sub>)O<sub>2</sub> for Lithium(-ion) batteries with outstanding cycling stability and enhanced lithiation kinetics. *Adv. Energy Mater.* **2018**, *18*, 1573.
27. Jiang, X.D.; Yuan, Z.T.; Liu, J.X.; Jin, X.; Jin, L.Y.; Dong, P.; Zhang, Y.J.; Yao, Y.N.; Cheng, Q.; Liu, C.; et al. Effects of LaPO<sub>4</sub> coating on the performance of LiNi<sub>0.5</sub>Co<sub>0.2</sub>Mn<sub>0.3</sub>O<sub>2</sub> cathode material for lithium ion batteries. *Int. J. Electrochem. Sci.* **2018**, *13*, 2341–2354. [[CrossRef](#)]
28. Feng, Z.; Rajagopalan, R.; Sun, D.; Tang, Y.; Wang, H. In-situ formation of hybrid Li<sub>3</sub>PO<sub>4</sub>-AlPO<sub>4</sub>-Al(PO<sub>3</sub>)<sub>3</sub> coating layer on LiNi<sub>0.8</sub>Co<sub>0.1</sub>Mn<sub>0.1</sub>O<sub>2</sub> cathode with enhanced electrochemical properties for lithium-ion battery. *Chem. Eng. J.* **2020**, *382*, 122959. [[CrossRef](#)]
29. Yue, C.C.; Shi, B.Z.; Guo, C.L. Improving the electrochemical performance of LiNi<sub>0.6</sub>Co<sub>0.1</sub>Mn<sub>0.3</sub>O<sub>2</sub> cathode at high cutoff voltage by dual functions of Y(PO<sub>3</sub>)<sub>3</sub> modification. *Solid State Ionics* **2021**, *368*, 115674. [[CrossRef](#)]
30. Zhang, H.Z.; Qiao, Q.Q.; Li, G.R.; Gao, X.P. PO<sub>4</sub><sup>3-</sup> polyanion-doping for stabilizing Li-rich layered oxides as cathode materials for advanced lithium-ion batteries. *J. Mater. Chem. A* **2014**, *2*, 7454. [[CrossRef](#)]
31. Gao, S.; Wang, L.J.; Zhou, C.Y.; Guo, C.L.; Zhang, J.L.; Li, W. In-situ construction protective layer and phosphate doping synergistically improve the long-term cycle stability of LiNi<sub>0.6</sub>Co<sub>0.1</sub>Mn<sub>0.3</sub>O<sub>2</sub>. *Chem. Eng. J.* **2021**, *426*, 131359. [[CrossRef](#)]
32. Senthil, C.; VEDIAPPAN, K.; Nanthagopal, M.; Kang, H.S.; Gnanamuthu, R.; Lee, C.W. Thermochemical conversion of eggshell as biological waste and its application as a functional material for lithium-ion batteries. *Chem. Eng. J.* **2019**, *372*, 765–773. [[CrossRef](#)]
33. Ran, Q.W.; Zhao, H.Y.; Shu, X.H.; Hu, Y.Z. Enhancing the electrochemical performance of Ni-rich layered oxide cathodes by combination of the gradient doping and dual-conductive layers coating. *ACS Appl. Energy Mater.* **2019**, *2*, 3120–3130. [[CrossRef](#)]
34. Yi, T.F.; Li, Y.M.; Cai, X.D.; Yang, S.Y.; Zhu, Y.R. Fe-stabilized Li rich layered Li<sub>1.2</sub>Mn<sub>0.56</sub>Ni<sub>0.16</sub>Co<sub>0.08</sub>O<sub>2</sub> oxide as a high performance cathode for advanced lithium-ion batteries. *Mater. Today Energy* **2017**, *4*, 25–33. [[CrossRef](#)]
35. Zhao, T.L.; Chen, S.; Li, L.; Zhang, X.F.; Chen, R.J.; Belharouak, I.; Wu, F.; Amine, K. Synthesis, characterization, and electrochemistry of cathode material Li[Li<sub>0.2</sub>Co<sub>0.13</sub>Ni<sub>0.13</sub>Mn<sub>0.54</sub>]O<sub>2</sub> using organic chelating agents for lithium-ion batteries. *J. Power Sources* **2013**, *228*, 206–213. [[CrossRef](#)]
36. Xiong, Y.K.; Chang, S.H.; Li, Y.J.; Zheng, J.C.; Ren, X.G.; Tan, Z.L.; Xi, X.M.; Yang, J.C.; Liu, S.W.; Wang, S. Enhancing surface and internal structural stability of LiNi<sub>0.8</sub>Co<sub>0.1</sub>Mn<sub>0.1</sub>O<sub>2</sub> by yttrium phosphate dual effects. *J. Alloys Compd.* **2022**, *894*, 162155. [[CrossRef](#)]
37. Ran, Q.W.; Zhao, H.Y.; Hu, Y.Z.; Hao, S.; Shen, Q.Q.; Liu, J.T.; Li, H.; Xiao, Y.; Li, L.; Wang, L.P.; et al. Multifunctional integration of double-shell hybrid nanostructure for alleviating surface degradation of LiNi<sub>0.8</sub>Co<sub>0.1</sub>Mn<sub>0.1</sub>O<sub>2</sub> cathode for advanced Lithium-ion batteries at high cutoff voltage. *ACS Appl. Mater. Interfaces* **2020**, *12*, 9268–9276. [[CrossRef](#)]
38. Wu, K.; Jiao, J.Y.; Li, N.; Wang, M.; Jia, G.F.; Lee, Y.L.; Dang, R.B.; Deng, X.; Xiao, X.L.; Wu, Z.J. Revealing the multiple influences of Zr substitution on the structural and electrochemical behavior of high Nickel LiNi<sub>0.8</sub>Co<sub>0.1</sub>Mn<sub>0.1</sub>O<sub>2</sub> cathode material. *J. Phys. Chem. C* **2021**, *125*, 10260–10273. [[CrossRef](#)]
39. Yang, S.; Shadik, Z.; Wang, W.; Yue, X.; Xia, H.; Bak, S.; Du, Y.; Li, H.; Fu, Z. An ultrathin solid-state electrolyte film coated on LiNi<sub>0.8</sub>Co<sub>0.1</sub>Mn<sub>0.1</sub>O<sub>2</sub> electrode surface for enhanced performance of lithium-ion batteries. *Energy Stor. Mater.* **2022**, *45*, 1165–1174. [[CrossRef](#)]
40. Zhao, Z.R.; Li, H.P.; Zheng, Z.Y.; Zheng, L.Y.; Yan, Y.W. Improved thermal shock and corrosion resistance of α-Al<sub>2</sub>O<sub>3</sub>/AlPO<sub>4</sub> coating with PAA addition. *Surf. Coat. Technol.* **2021**, *414*, 127115. [[CrossRef](#)]
41. Zhang, M.; Zhao, H.; Tan, M.; Liu, J.; Hu, Y.; Liu, S.; Shu, X.; Li, H.; Ran, Q.; Cai, J.; et al. Yttrium modified Ni-rich LiNi<sub>0.8</sub>Co<sub>0.1</sub>Mn<sub>0.1</sub>O<sub>2</sub> with enhanced electrochemical performance as high energy density cathode material at 4.5 V high voltage. *J. Alloys Compd.* **2019**, *774*, 82–92. [[CrossRef](#)]
42. Tang, W.; Peng, Z.; Shi, Y.; Xu, S.; Shuai, H.; Zhou, S.; Kong, Y.; Yan, K.; Lu, T.; Wang, G. Enhanced cyclability and safety performance of LiNi<sub>0.6</sub>Co<sub>0.2</sub>Mn<sub>0.2</sub>O<sub>2</sub> at elevated temperature by AlPO<sub>4</sub> modification. *J. Alloys Compd.* **2019**, *810*, 151834. [[CrossRef](#)]
43. Deylami, M.R.; Javanbakht, M.; Omidvar, H. Enhanced performance of layered Li<sub>1.2</sub>Mn<sub>0.54</sub>Ni<sub>0.13</sub>Co<sub>0.13</sub>O<sub>2</sub> cathode material in Li-ion batteries using nanoscale surface coating with fluorine-doped anatase TiO<sub>2</sub>. *Solid State Ionics* **2019**, *331*, 74–88. [[CrossRef](#)]
44. Zhang, X.; Xie, X.; Yu, R.; Zhou, J.; Huang, Y.; Cao, S.; Wang, Y.; Tang, K.; Wu, C.; Wang, X. Improvement of the cycling stability of Li-rich layered Mn-based oxide cathodes modified by nanoscale LaPO<sub>4</sub> coating. *ACS Appl. Energy Mater.* **2019**, *2*, 3532–3541. [[CrossRef](#)]
45. Cho, J.; Kim, T.J.; Kim, J.; Noh, M.; Park, B. Synthesis, thermal and electrochemical properties of AlPO<sub>4</sub>-coated LiNi<sub>0.8</sub>Co<sub>0.1</sub>Mn<sub>0.1</sub>O<sub>2</sub> cathode materials for a Li-ion cell. *J. Electrochem. Soc.* **2004**, *151*, 1899–1904. [[CrossRef](#)]
46. Peng, Z.D.; Li, T.F.; Zhang, Z.Y.; Du, K.; Hu, G.R.; Cao, Y.B. Surface architecture decoration on enhancing properties of LiNi<sub>0.8</sub>Co<sub>0.1</sub>Mn<sub>0.1</sub>O<sub>2</sub> with building bi-phase Li<sub>3</sub>PO<sub>4</sub> and AlPO<sub>4</sub> by Al(H<sub>2</sub>PO<sub>4</sub>)<sub>3</sub> treatment. *Electrochim. Acta* **2020**, *338*, 135870. [[CrossRef](#)]
47. He, R.; Bai, X.; Wei, A.J.; Zhang, L.H.; Liu, P.; Liu, Z.F. Y<sub>2</sub>O<sub>3</sub> modification on nickel-rich LiNi<sub>0.8</sub>Co<sub>0.1</sub>Mn<sub>0.1</sub>O<sub>2</sub> with improved electrochemical performance in lithium-ion batteries. *J. Rare Earths* **2022**, *40*, 309–317. [[CrossRef](#)]
48. Zhu, W.C.; Huang, X.; Liu, T.T.; Xie, Z.Q.; Wang, Y.; Tian, K.; Bu, L.M.; Wang, H.B.; Gao, L.J.; Zhao, J.Q. Ultrathin Al<sub>2</sub>O<sub>3</sub> coating on LiNi<sub>0.8</sub>Co<sub>0.1</sub>Mn<sub>0.1</sub>O<sub>2</sub> cathode material for enhanced cycle ability at extended voltage ranges. *Coatings* **2019**, *9*, 92. [[CrossRef](#)]

49. Li, T.; Li, D.; Zhang, Q.; Gao, J.; Zhang, L.; Liu, X. Improving fast charging-discharging performances of Ni-rich  $\text{LiNi}_{0.8}\text{Co}_{0.1}\text{Mn}_{0.1}\text{O}_2$  cathode material by electronic conductor  $\text{LaNiO}_3$  crystallites. *Materials* **2022**, *15*, 396. [[CrossRef](#)]
50. Ma, B.; Huang, X.; Liu, Z.; Tian, X.; Zhou, Y.  $\text{Al}_2\text{O}_3$  coated single-crystalline hexagonal nanosheets of  $\text{LiNi}_{0.6}\text{Co}_{0.2}\text{Mn}_{0.2}\text{O}_2$  cathode materials for the high-performance lithium-ion batteries. *J. Mater. Sci.* **2022**, *57*, 2857–2869. [[CrossRef](#)]
51. Zhu, M.; Li, J.; Liu, Z.; Wang, L.; Kang, Y.; Dang, Z.; Yan, J.; He, X. Preparation and electrochemical properties of  $\text{LiNi}_{2/3}\text{Co}_{1/6}\text{Mn}_{1/6}\text{O}_2$  cathode material for Lithium-Ion Batteries. *Materials* **2021**, *14*, 1766. [[CrossRef](#)] [[PubMed](#)]